Image Projection with Nonlinear Optics

The nonlinear optical process of conjugate wavefront generation by degenerate four-wave mixing can project images in a manner akin to conventional optical systems. The underlying physics is quite different, and the difference allows higher resolution over larger useful fields. This article reviews the basics of conjugate wavefront generation and its relationship to holography, and proposes applications in fine-line lithography. Initial experiments confirm the predicted advantages but also point out inadequacies in present-day nonlinear optics technology.

Introduction

Since the invention of the camera obscura in the sixteenth century, the primary purpose of optics has been to produce images: patterns of light intensity that somehow capture the characteristics of objects that exist somewhere else. While optical systems have increased in sophistication since the sixteenth century, the underlying physical processes that allow the formation of images—the laws of rectilinear propagation, reflection, and refraction—have not changed. A great deal of sophisticated engineering effort has been expended to overcome the limitations of conventional imaging systems imposed by diffraction, aberrations, and other annoying but well-understood phenomena.

Very recently, a new optical effect has been discovered which forms images as the result of an entirely different kind of process. Termed conjugate wavefront generation by degenerate four-wave mixing, this phenomenon can form images that are mathematically identical replicas of the original objects [1-3]. The effect is intrinsically nonlinear; it relies on the interaction of light waves with one another in a medium to form the image, rather than the interactions of light with material surfaces, as is the case with conventional optics. High intensity is required to make the process reasonably efficient but sufficient intensities are readily available from a number of laser sources.

Moreover, the wavefront-conjugation process has the capability of correcting many of the aberrations present in a conventional optical system. High-quality images can thus be projected through low-quality optics and nonuniform, highly aberrating media. Because ultraviolet and vacuum ultraviolet wavelengths can be used and because the numerical aperture of wavefront-conjugation systems can be made quite large, the resolution achievable by this technology is superior to that of any other type of optical system [4, 5]. In a well-designed wavefront conjugator, the full resolution can be available over a field centimeters in diameter. Such systems may be appropriate as replacements for the 1:1 imaging systems used for fine-line photolithography in microcircuit manufacture [6]. A great deal of sophisticated engineering and some fascinating materials science must take place, however, before wavefront-conjugation exposure tools become practical. Similar efforts will be needed to develop the proposed military and communications aspects of wavefront conjugation.

It is no small challenge to produce integrated circuits with submicron structures economically. Current optical techniques are approaching their fundamental limits. The more exotic electron-beam and x-ray (including synchrotron) radiation technologies have not yet become compatible with mass production [7]. However, the prosperity of the computer industry has largely been based on our continuing ability to manufacture hardware with more capability at less cost. In terms of fine-line lithography, more capability at less cost translates into more and smaller circuitry at equal or increasing yields. Photolithography has been remarkably successful in this regard, evolving to meet every challenge

Copyright 1982 by International Business Machines Corporation. Copying is permitted without payment of royalty provided that (1) each reproduction is done without alteration and (2) the *Journal* reference and IBM copyright notice are included on the first page. The title and abstract may be used without further permission in computer-based and other information-service systems. Permission to *republish* other excerpts should be obtained from the Editor.

without the disruption of a complete technological revolution. Thus any innovation that promises to extend this evolutionary progress into the VLSI (very large scale integration) era is an important innovation indeed [8].

Figure 1 shows a typical scheme for projecting an image by wavefront conjugation. Two pump beams traveling in opposite directions pass through a medium with an index of refraction that depends on light intensity. Light from an object point O interacts with these waves in the medium to generate new wavefronts (indicated by dashed lines) that propagate back towards the object point O. These wavefronts are phase-conjugate replicas of the object waves initially emitted from the object point. Phase-conjugate replica waves have the same three-dimensional phase fronts and relative amplitudes as the object waves, but propagate through space as if time were reversed. Thus, while the object wave goes from the object O into the wavefront conjugator medium, the phase-conjugate replica propagates back from the medium to O. A partly transmitting mirror at plane B-B can intercept part of this backwards-propagating wave and reflect it to an image point I. Because of the time-reversal symmetry between the object and phase-conjugate waves, the pattern of intensities at the image identically reproduces that at the object. An aberrating medium placed between the beam splitter and the conjugating medium has no effect on the image. The time-reversal symmetry inherent in the conjugation process requires that the aberrator remove the distortions from the conjugate wave that it imposed on the object wave [1-4].

The process of wavefront conjugation is related to holography and nonlinear optical phenomena such as self-focusing and coherent anti-Stokes Raman spectroscopy [9-13]. It differs from the former mostly in that image formation is nearly instantaneous and does not require development of a light-sensitive recording medium. For that reason, some early workers termed this process dynamic or real-time holography. The second section of this paper explores the relationships between conjugate wavefront generation and more conventional holographic techniques. The third section introduces the third-order nonlinear susceptibility in terms of which interactions among light waves are most easily described. It also relates wavefront conjugation to other nonlinear optical phenomena. The fourth section summarizes the results obtained in our project to demonstrate the fine-line lithography capabilities of wavefront conjugation, and the final section indicates directions for future research and development efforts.

Conjugate wavefront generation as real-time holography

Conventional holography records three-dimensional images on photographic emulsion without the use of lenses. After

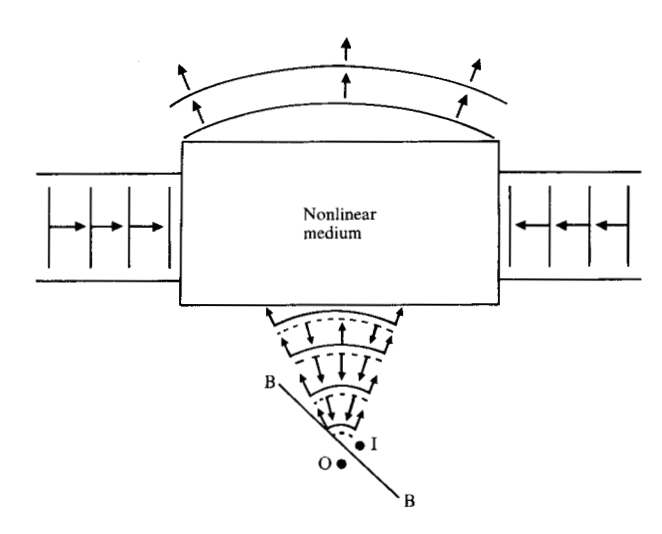


Figure 1 A prototypical system for conjugate wavefront generation by degenerate four-wave mixing. The two pump waves propagate horizontally. The object wave diverges from point O and the image wave (---) initially converges toward point O, but is reflected to point I by the partially transparent mirror B-B.

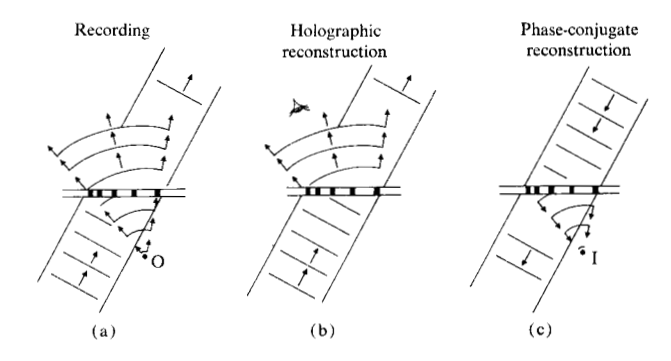


Figure 2 Holographic (a) recording and (b) reconstruction. (c) Replication of a real, phase-conjugate image by this same hologram plate.

development, the images are reconstructed from the information encoded on the emulsion. The essence of this process is diagrammed in Fig. 2. In the recording stage, the photosensitive emulsion is illuminated with a reference wave (propagating from lower left or upper right) with plane phase fronts and relatively uniform intensity. Light originating from an object point O interferes with this reference wave, making light and dark fringes. These fringes encode all of the information about the object that is carried by the light [9]. The photosensitive emulsion exposes more heavily at the maxima of the interference pattern and remains relatively unexposed at the minima, thus recording the information carried by the object wave.

In conventional holography, the photosensitive emulsion must be developed, causing more grains of silver to coalesce in the exposed regions and fewer in the unexposed areas. In holographic media the individual grains are very small, but under a microscope, the developed fringe patterns are readily visible as dark and light bands. The difference in opacity due to the varying density of silver grains can be thought of as a variation in the imaginary part of the refractive index of the developed emulsion. Holographers term such a pattern an absorption hologram. Techniques exist for removing the silver grains, and thus, for making the hologram completely transparent. The regions from which the silver is removed remain empty and have a lower index of refraction than the surrounding media. Variation in the index of refraction remains even in a completely transparent hologram. Such phase holograms have higher efficiency than the absorption type [14].

The most common process for reconstruction of a virtual image from a developed hologram is shown in Fig. 2(b). The developed hologram is illuminated with a reconstructing wave identical to the reference wave used to record the hologram. The reconstructing wave propagates in the same direction as the original reference wave. The variations of the real or imaginary parts of the index of refraction of the medium modulate the wavefront and lead to scattering. The perturbed wavefront can be decomposed mathematically into three terms, two of which are the original reference wave and a replica of the object wave. If the holographic medium is much thicker than the fringe spacing, only these two components matter.

One can then imagine that the replica of the object wave is produced by Bragg scattering of the reconstructing beam by the many parallel layers of varying refractive index produced by the original fringe pattern. In any case, the holographic replica wave scattered from the medium is identical to the portion of the object wave that would have been transmitted through the emulsion. An observer looking through the hologram would not be able to determine whether he was viewing an object on the other side or merely an image reconstructed from the information encoded in the hologram. The image seen by the observer is, however, virtual; a detector placed where the image appeared to be would not find any light.

Real images can be produced from thick holograms by the reconstruction process shown in Fig. 2(c). Here, the reconstructing wave is the *phase conjugate* of the original reference wave. The same modulation and scattering phenomena that gave rise to the virtual image in Fig. 2(a) now produce a phase-conjugate replica of the object wave. Thus, Figs. 2(a) and (c) are identical except for the arrows indicating the directions of light propagation. The phase-conjugate replica

waves converge, forming a real image at the surface where the object had been. This reconstruction geometry is not used extensively because the image formed has an unusual property: viewed from behind it appears inside out, or *pseudoscopic*. If the original object had been a person's head with the face illuminated, the phase-conjugate image would look like a face viewed from the inside through a transparent skull. In some optical applications, perfect replication of an intensity pattern is not desirable.

In conjugate wavefront generation by degenerate fourwave mixing, all three steps of the holographic process recording, development, and reconstruction—occur simultaneously [2, 3]. The media used have the property that their indices of refraction depend on the incident intensity. Thus, the presence of an interference between the object wave and one pump wave directly produces planes of index variation that Bragg-scatter the other pump wave into a phaseconjugate replica of the object wave. In most systems there is complete symmetry between the pump waves; thus, there are actually two holograms and two images being produced and reconstructed simultaneously. As in holography, it is necessary that the object wave and the pump used as a reference be mutually coherent. It is not necessary that the other pump be coherent with the object wave, but it is sometimes advantageous. To achieve the theoretical image fidelity, the two pump waves must be phase conjugates of one another.

Holography was once considered for use as an imaging technology for fine-line lithography, but it was found to suffer from three serious disadvantages [15]. First, reproducing an image that is identical to the object requires that the reconstructing beam be exactly the phase conjugate of the original reference beam. The angle between the hologram and the reconstructing beam must be exactly right: otherwise, there will be distortions and magnification. Second, the developing process required by most holographic media causes those media to physically distort, often swelling by several percent. This distortion alters the fringe spacing and distorts the image unacceptably. Finally, the holographic process records too much information, such as imperfections in the beams used to illuminate the object, the position of scratches and dust particles, surface irregularities, etc. This information appears in the image as speckle, which is a 100% modulation of the light intensity of the image [16]. The average physical size of a spot on a speckle pattern approximates the resolution of the optical system. Suppressing this speckle noise in holography reduces both resolution and efficiency.

Because wavefront conjugation is a real-time process, these disadvantages of holography are readily overcome. Simple alignment procedures ensure the required symmetry between the reference and reconstructing pump beams. There is no development to cause distortion. And speckle can be eliminated either by use of uniphase wavefronts to illuminate transmission objects or by purposely scrambling the phase of the illumination during an exposure [5, 17].

Both holography and wavefront conjugation are capable of resolution superior to that of conventional projection optics. The minimum feature size that can be reproduced in an image depends on the range of angles within which waves can be made to converge at a point. If all waves within a cone of angle θ converge correctly at an image point, the minimum feature size of that image is

$$\Lambda = \frac{2}{\pi} \frac{\lambda}{\sin \theta},\tag{1}$$

and $\sin \theta$ is the numerical aperture [18]. Lenses which must image small objects (i.e., microscope objectives) can be made with numerical apertures approaching unity. However, the resolution thus obtained is available only in a region a few microns in diameter. Beyond that distance, aberrations due to the sharply curved surfaces of the lens distort the image. Such lenses are not suitable for fine-line lithography. To date, the best microprojection lenses have numerical apertures less than 0.35 and a usable field size of ≈1 cm. Holographic and wavefront conjugation imaging systems can collect light over a numerical aperture of 0.7, resulting in a doubling of the resolution. Because all surfaces are plane, the field size can be made as large as necessary. Moreover, available lasers and materials allow images to be projected using deep uv and vacuum uv radiation. The use of these shorter wavelengths can again double the resolution, providing reasonable depth of focus for images with submicron features.

Conjugate wavefront generation as nonlinear optical mixing

Some of the earliest experiments performed with lasers showed that new frequencies could be generated as a result of nonlinear interactions between light waves in certain media. These effects demonstrated that Maxwell's description of light-matter interactions in terms of a linear coupling was incomplete. At the intensities characteristic of laser beams, the dielectric polarization had to be expressed as a power series in optical amplitude:

$$P_{i} = \chi_{ij} E_{j} + \chi_{ijkl}^{(2)} E_{j} E_{k} + \chi_{ijkl}^{(3)} E_{j} E_{k} E_{l} + \cdots$$
 (2)

Only the first term in (2) is required to describe all linear optics. The higher-order terms give rise to nonlinear effects such as harmonic generation and nonlinear mixing [10,11]. The coefficients of these higher-order terms are called nonlinear optical susceptibility tensors. In most materials, $\chi^{(2)}$ vanishes by symmetry, leaving $\chi^{(3)}$ as the lowest nonvanishing nonlinearity. In the usual approximation, the fields are

expanded in spatial and temporial Fourier components and Eq. (2) is applied to appropriate combinations of these components. Such a treatment is rigorous only when the rate of change of the amplitudes is slow compared to the relaxation times of the nonlinear media [19, 20]. Also, terms above $\chi^{(3)}$ are usually ignored even though the actual dielectric polarization can be specified analytically in many simple cases.

Writing the electric fields as

$$E_{j}(\vec{r},t) = \frac{1}{2} E_{j} e^{i(\vec{k}_{j} \cdot \vec{r} - \omega_{j}t)} + \frac{1}{2} E_{j}^{*} e^{-i(\vec{k}_{j} \cdot \vec{r} - \omega_{j}t)},$$
 (3)

where \vec{k} is the wave vector, ω is the frequency, and t is the time, it is easy to see how Eq. (2) can give rise to polarizations at the sum and difference frequencies of the incident radiation. By convention, $\chi^{(3)}$ is written with four frequency arguments,

$$\chi_{ijkl}^{(3)}(\omega_i, \omega_i, \omega_k, \omega_l),$$

with the restriction that $\omega_i + \omega_j + \omega_k + \omega_l = 0$. The dielectric polarization density in (2) radiates according to Maxwell's wave equation:

$$\nabla \times \nabla \times E_i + \frac{\varepsilon_{ij} \, \partial^2}{c^2 \, \partial t^2} E_j = -\frac{4\pi}{c^2} \frac{\partial^2}{\partial t^2} P_i \,. \tag{4}$$

The solution of (4) in regions larger than a few wavelengths implies that the radiated amplitude E_i can be appreciable only if the wave-vector matching condition,

$$\left|\vec{k}_{i}-(\vec{k}_{j}+\vec{k}_{k}+\vec{k}_{l})\right|\approx0,$$
 (5)

is fulfilled.

These simple considerations are the basis of nonlinear optics. The third-order nonlinear susceptibility is a material parameter, similar to the index of refraction. Like the index of refraction, it is complex and shows dispersion and resonances [13]. While $\chi^{(3)}$ can in principle be calculated using third-order quantum-mechanical perturbation theory, in practice that calculation is even more difficult than experimentally measuring the nonlinearity. Over the last decade, considerable effort has been expended in studying $\chi^{(3)}$ and its resonances. A number of useful spectroscopic tools have resulted [13, 21, 22].

The presence of $\chi^{(3)}$ also implies an intensity dependence to the index of refraction:

$$n(\omega) = n_0 + n_1 |E(\omega)|^2, \tag{6}$$

where the intensity $I = (cn/4\pi) |E(\omega)|^2$ and where $n_2 = (12\pi/n_0)\chi_{1111}^{(3)}(-\omega, \omega, \omega, -\omega)$. This nonlinear refraction phenomenon leads to a variety of dramatic and generally undesirable effects, notably self-focusing, but it also underlies the common forms of conjugate wavefront generation. In typical

163

materials $\chi^{(3)}$ and n_2 are quite small: $\chi^{(3)} \approx 10^{-14}$ esu, $n_2 \approx 10^{-12}$ esu $\approx 10^{-10}$ (W/cm²)⁻¹. (The esu dimensions for $\chi^{(3)}$ and n_2 are cm³/erg = 10 m³/J). However, at the intensities of pulsed lasers, these values are quite sufficient. In certain materials the nonlinearities are much greater, and large effects can be obtained even with cw lasers. As a rule of thumb, the intensity of a wave generated by a nonlinear optical interaction is roughly

$$I_{\rm s} \approx 50 \left\{ \frac{\varrho_{\rm eff}}{\lambda} \frac{n_2 E_1 E_2}{n_0} \right\}^2 I_0, \tag{7}$$

where λ is the wavelength, ℓ_{eff} is the effective length of the nonlinear medium, E_1 and E_2 are the pump electric fields, and I_0 is the intensity of the object wave.

In a typical conjugate-wavefront-generation geometry, the pump waves propagate through the medium with wave vectors $\vec{k}_1 = \vec{k}_p$, $\vec{k}_2 = -\vec{k}_p$ and the object wave contains a variety of wave vectors \vec{k}_0 and has amplitude E_0 . The magnitudes of all of the wave vectors are $\omega n_i/c$, where n_i is the index of refraction for the *i*th polarization. The term in Eq. (2) which gives rise to the conjugate wave is

$$P = 6\chi_{1111}(-\omega, \omega, \omega, -\omega)E_1E_2E_0^{\dagger}e^{i(\vec{k}_s\cdot\vec{r}-\omega t)}.$$
 (8)

According to (5), $\vec{k}_s = -\vec{k}_0$, where k_s is the wave vector of the generated signal. Equations (3) and (4) imply that the radiated wave propagates as

$$E_{\rm s} = \frac{\eta}{2} \, E_0 e^{i (\vec{k}_0 \cdot \vec{r} + \omega t)} + \frac{\eta}{2} \, E_0^* e^{-i (\vec{k}_0 \cdot \vec{r} + \omega t)}, \label{eq:energy}$$

which resembles (3) with the parameters of the object wave (i.e., E_0 and k_0) inserted except that the sign of t has been reversed and an efficiency factor η that depends on $\chi^{(3)}$ multiplies the amplitude.

It is instructive to write Eq. (8) in terms of the dot products of the incident fields:

$$\hat{P} = \{ \mathcal{A}(\vec{E}_2 \cdot \vec{E}_0^*) \vec{E}_1 + B(\vec{E}_1 \cdot \vec{E}_0^*) \vec{E}_2
+ C(\vec{E}_1 \cdot \vec{E}_2) E_0^* \} e^{i(\vec{k}_p \cdot \vec{r} = \omega t)}.$$
(9)

The first term corresponds to scattering the pump wave E_1 by the fringe pattern formed between the object wave and pump E_2 ; the second term corresponds to scattering E_2 by a fringe pattern formed by E_1 and E_0 [23]. Nothing in this treatment requires that these fringe patterns be stationary; so long as they move more slowly than the response time of the nonlinear medium, the efficiency and the image quality are unaffected. Equation (9), however, makes clear that the dynamics behind this sort of wavefront conjugation occurs on a frequency scale well below optical frequencies.

The third term has no such simple interpretation. It results from a parametric mixing process that becomes

resonant when the energy of two photons becomes resonant with an energy level of the medium. No fringe patterns are involved; the simplest interpretation of this term is that it reflects the simultaneous destruction of one photon from each pump beam with the consequent creation of photons in the object wave and the conjugate wave.

It is a straightforward exercise in integration to show that the polarization density in (8) radiates a wave that reproduces the object wave and images to an exact replica of the source [1, 24]. If there is no speckle in the intensity pattern at the object, there will be none at the image. The minimum feature size can be shown to be essentially that given in (1).

Unlike the previous treatment in terms of holography, a description of wavefront conjugation as nonlinear mixing allows discussion of effects which tend to compromise the quality of the image. In particular, self-focusing of the pump beams might break the perfect phase-conjugate symmetry necessary for image fidelity. Since laser beams are more intense in the center than at the edge, nonlinear refraction tends to alter the phase velocity across the beam profile. After a sufficient length of propagation through a nonlinear medium, the resulting phase front curvature can turn a plane wave into a sharply focused or divergent spherical wave. Since this effect is formally the same order in the incident amplitudes as conjugate wavefront generation, it probably limits the efficiency of any high-resolution projection device [12]. Fortunately, the designers of super-high-power lasers have invented schemes to minimize self-focusing by making laser beams uniform in intensity over most of their diameters [25]. At very high intensities, even a uniform beam becomes unstable; it tends to break up into numerous converging "beamlets." This instability imposes a fundamental limit on the pump intensity in wavefront conjugation.

Higher-order nonlinear processes might radiate waves in undesired directions and thereby degrade the image. In fact, most higher-order nonlinear processes seem to have no significant effect until well after the limit imposed by self-focusing [26, 27]. One exception to this rule concerns saturation of the nonlinearity, which occurs when the intensity in one region of the medium becomes so great that the dielectric polarization cannot become large enough to fulfill (8). This effect can distort the image through the loss of necessary Fourier components [28]. The solution is to alter the design of the device to eliminate such hot spots.

There is a considerable literature on third-order nonlinearities which can assist in choosing promising materials for the conjugator medium. Figure 3 illustrates eight of the physical processes leading to an intensity-dependent change in the index of refraction that can be used for wavefront conjugation. In Fig. 3(a), molecules in a Kerr fluid reorient

164

to align their anisotropic molecular polarizabilities with the field. In the presence of a strong optical field, more molecules are aligned with the directions of their larger polarizabilities along the field; thus, the index of refraction increases [11]. For MBBA and other liquid crystals in their isotropic phases, $n_2 \approx 10^{-8}$ esu, but the relatively long relaxation time (several tens of nanoseconds) reduces the efficiency [29]. Figure 3(b) shows the process of two-level saturation of an absorbing material. When the material is in the excited state, the absorption is bleached and a transient absorption hologram can result [30]. Figure 3(c) shows a more sophisticated variation in which atoms or molecules decay into a metastable state which does not interact with the radiation. Here, optical pumping leads to long-lived changes in absorption and dispersion. Until the molecules return to the ground level, the absorption and dispersion are reduced [31]. For sodium vapor, the metastable state is a nuclear spin state that relaxes very slowly; the nonlinearity is $n_2 \approx 10^{-4}$ esu at a density of 10¹³ atoms/cm³ [32]. When the radiation is tuned just off a strong resonance, the light shift (optical Stark effect or electronic Kerr effect) can displace the energy levels, as shown in Fig. 3(d), altering the dispersion. Nonlinearities as large as $n_2 = 10^{-8}$ esu have been seen in sodium, and the relaxation time can be made as short as necessary. Using sodium, Bloom, Liao, and Economou obtained conjugate waves 80 times stronger than the incident object wave [33].

Figure 3(e) shows the two-photon resonant parametric mixing process. In sodium, the nonlinear susceptibility is $n_2 = 10^{-10}$ esu at 10^{14} /cm³. The relaxation time is 30 ns [34]. In semiconductors, strong laser fields can produce enough free carriers to alter the plasma frequency, thus changing the index of refraction; see Fig. 3(f). In silicon, the nonlinearity is $n_2 = 10^{-6}$ esu at 1.06 μ m [35]. In photorefractive materials [Fig. 3(g)], light causes physical separation of mobile carriers from shallow traps (fixed charges) in regions of high intensity and deposits them in regions of lower intensity. The resulting charge separation produces a dc field which alters the index of refraction by means of the Pockels effect [36]. Very large efficiencies can result at very low intensities. The relaxation time, unhappily, is typically tens of seconds [5]. Finally, as shown in Fig. 3(h), optical (radiation) forces on the submicron particles in colloids and aerosols can be sufficient to push these particles into regions of high (or low) intensity. Since those regions then show an increased (or decreased) average index of refraction, wavefront conjugation results. The nonlinearity is typically n_2 = 10^{-6} /esu with a 400-ms relaxation time [37].

As long as it is, this list can hardly be considered comprehensive. Conjugate wavefront generation due to temperature gratings, photochemical and photophysical effects, and many other phenomena continue to be reported.

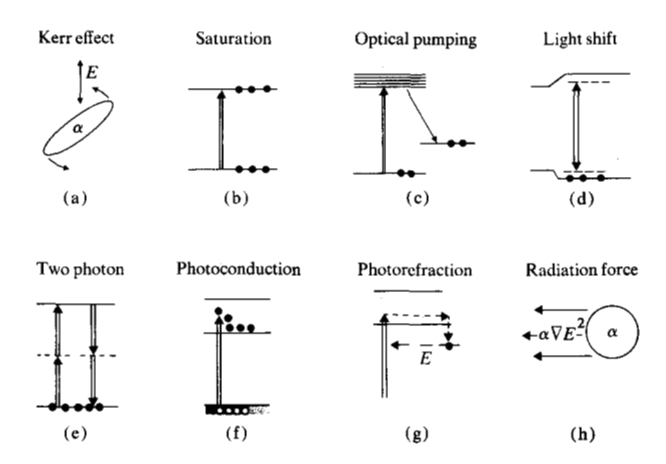


Figure 3 Eight processes leading to an intensity-dependent change in the index of refraction that can be used for wavefront conjugation. See the text for details.

Experiments in fine-line lithography

Early treatments of conjugate wavefront generation were unclear as to the factors limiting the resolution [1-4]. In 1979 we began a series of experiments intended to demonstrate that features as small as one wavelength could be imaged by degenerate four-wave mixing [4]. In the original apparatus the conjugator medium was a rectangular block of ruby through which 514.5-nm pump waves propagated in opposite directions. The object was a pattern of lines and gaps prepared by vector-scanned electron-beam lithography and illuminated from behind by a diverging laser beam. A beam-splitter cube collected the light incident in a cone angle of 40° and transmitted it into the conjugator medium. A high-power microscope magnified the image projected by the conjugator and permitted it to be photographed. The conjugator itself was 10 × 15 mm in size.

With this apparatus we were easily able to image patterns of five 1- μ m lines separated by 1- μ m gaps, as well as a variety of larger structures; 0.5- μ m lines with 0.5- μ m gaps were visible through the microscope but could not be photographed because of excessive vibration. The efficiency of the device was dismal, less than 0.001%, but that was to be expected from the known poor efficiency of ruby as a conjugator material and from the relatively low laser power. Still, the expected resolution had been demonstrated, and the usable field size was 4 mm across, which was 40% of the aperture of the beam splitter. The late John Hubbard developed a rigorous procedure for estimating the resolution of any such device [24].

To achieve brighter images over larger areas, the wavefront conjugator shown in Fig. 4 was assembled. The nonlinear medium was LiNbO₃, a photorefractive material that is transparent at 413.1 nm. This wavelength is short enough to

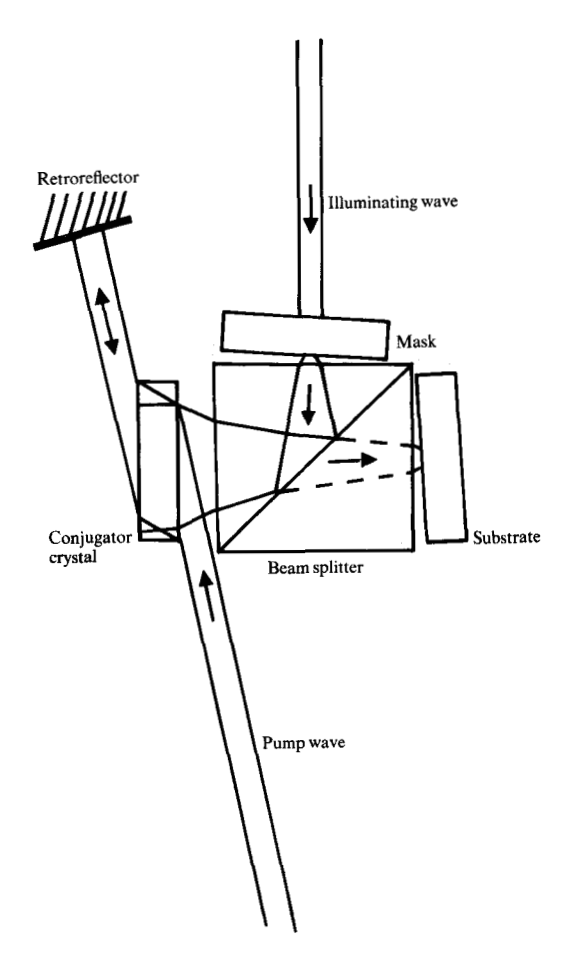


Figure 4 The wavefront conjugation projection system used for experiments in photolithography. The LiNbO₃ conjugator crystal was $25 \times 25 \times 5$ mm, with its optical axis in the plane of the diagram parallel to the long face of the crystal. All polarizations were in the plane of the diagram.

expose photoresist and can be produced by a Kr⁺ laser [5]. Photorefractive materials have high efficiencies at relatively low laser intensity levels, but the efficiency depends crucially on the spacing of the fringes in the interference pattern produced by the pump and object beams [38]. We found that the efficiency was essentially zero when the waves propagated at 90° to one another, yielding fringes with a spacing of 130 nm. Thus, we were forced to bring the pump wave into the crystal through the same face used for the object wave. The internal angle was reduced to 23° and the fringe spacing increased to 500 nm. The gap between the beam-splitter cube and conjugator crystal tended to reduce the numerical aperture, the usable field, and the efficiency; however, these disadvantages were not as great as the advantages to be gained by wavefront conjugation. The calculated numerical aperture was 0.60.

The light source for our experiment was a Spectra Physics 171-01 Kr⁺ laser. The 200-mW output of the laser was split

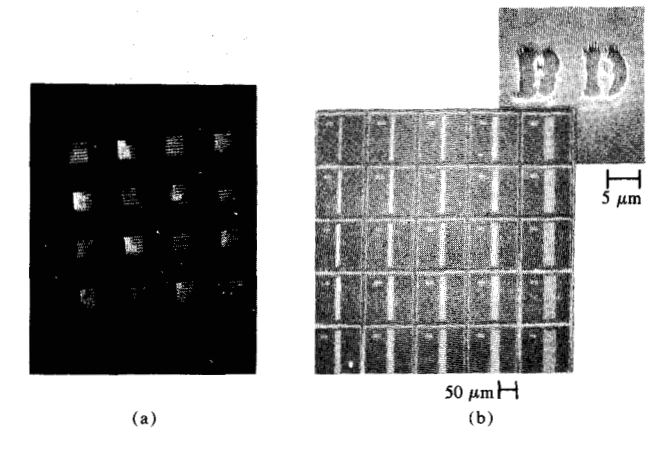


Figure 5 (a) A low-resolution micrograph of the photoresist pattern produced when the entire mask was projected onto a substrate using an expanded laser beam. The individual square chips are 0.8 mm on a side, with a center-to-center distance of 2 mm. (b) Scanning electron micrograph (SEM) of the major portion of one test chip. The linewidths (top to bottom) are 0.5, 0.75, 1.0, 1.5 and 2.0 μ m. The separation of the lines or gap widths (left to right) are 0.5, 0.75, 1.0, 2.0, and 4.0 μ m. Blowup: typical set of letters (here, BD) used to identify one portion of the resolution test pattern.

into a pump and an illuminating beam, with 70% of the power in the pump. The pump beam was expanded by a factor of about three, collimated by a telescope of simple lenses, and expanded in the vertical direction by another factor of three by refraction in a pair of 45° prisms oriented away from the angle of minimum deviation. The output of this anamorphic lens system was an elliptical Gaussian beam with semi-major and semi-minor axes of 7.5 and 2.5 mm, respectively. The curvature of the phase fronts was measured with a shearing interferometer, and the telescope was adjusted to make the fringes as straight as possible. The pump beam polarization was rotated into a horizontal plane with a double Fresnel rhomb, and the edges of the beam were clipped by rectangular apertures.

To within an accuracy of ± 5 mm, the path length for the illuminating wave between the initial beam splitter and the conjugator was the same as that for the pump wave. This accuracy was necessary because of the roughly 2.5-cm coherence length of our multi-mode laser. The illuminating beam polarization was rotated by a half-wave plate, and the horizontally polarized component of this wave was selected by a Glan-Thompson prism and used to illuminate the object. The intensity of the illuminating wave could be varied independently of the pump by rotating the half-wave plate. The illuminating beam was an expanded TEM $_{\infty}$ 0 uniphase laser mode, and speckle was thus suppressed by the high degree of coherence.

The images were projected onto flat glass substrates coated with *AZ-1350B or *AZ-1370 positive photoresists

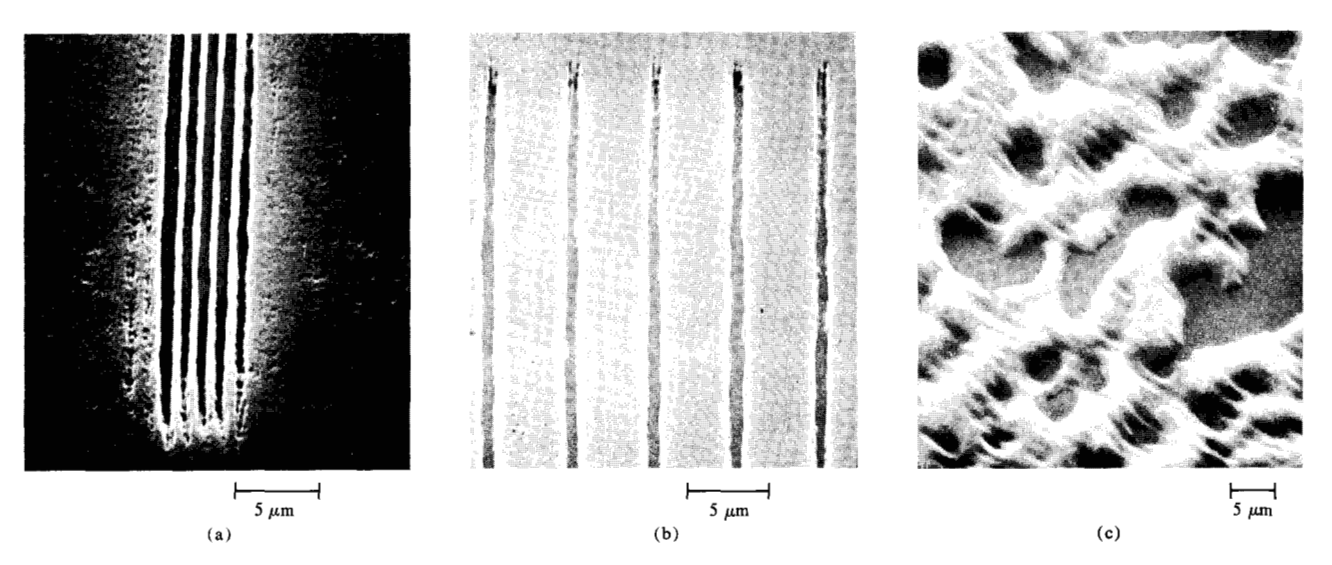


Figure 6 (a) and (b) Two of the finest sets of features projected and developed. At left are five 0.5- μ m lines separated by 0.5- μ m gaps, while at right are 0.5- μ m lines separated by 4.0- μ m gaps. The irregularities largely reflect the pattern on the mask drawn by vector-scanned electron-beam lithography. (c) SEM of a developed substrate produced by exposure to light scattered by a ground-glass screen. The screen, 1 cm away from the substrate, was illuminated with two 1.5-cm-diameter spots of 413-nm radiation separated by 1 cm. The rugged topography is typical of that produced by speckle. Standing wave patterns are absent because the substrate was baked briefly after development.

[39]. The resist coatings were 0.8 or 1.9 μ m in thickness, respectively. The substrates were positioned in the focal plane using Michaelson's white-light fringes in the interferometer formed by the substrate, mask, and beam-splitter cube. White light (filtered to remove the shorter wavelengths) was directed through the conjugator crystal into the beam-splitter cube. Light reflected by the mask and substrate was observed through the fourth face of the cube. When the mask and substrate were in planes nearly equidistant from the partially reflecting surface, brightly colored fringes appeared. The substrate could be leveled by maximizing the widths of these fringes, ultimately achieving a bulls-eye pattern. The substrate was then translated axially until the central colorless fringe appeared at the center. Since an axial translation of one half of a wavelength corresponds to a full fringe shift, this focusing procedure is accurate to 0.3 µm. In our best exposures, the mask and photoresist-coated substrate were within 0.5 mm of the face of the beam-splitter cube. An intensity monitor collected the light transmitted through the glass substrate and terminated the exposure automatically when the correct level of energy deposition was attained. Unhappily, the plane of best focus deviated from the zero fringe plane as a result of curvature of the beam-splitter surface. For our best beam splitter, actual focus was $15.0 \pm 0.5 \mu m$ behind the zero fringe plane.

In any image projection system, the depth of focus scales as the square of the minimum feature size. For a system with

a numerical aperture as high as ours, the depth of focus can be very small. By modeling the waves that focus to a spot of diameter Λ as a TEM $_{00}$ beam with the same diameter at its waist, the diameter of the beam varies with axial distance from focus as

$$\Lambda(z) = \Lambda \left\{ 1 + \frac{1}{1 - (2\lambda/\pi\Lambda)^2} \left[\frac{4}{\pi} \frac{\lambda z}{\Lambda^2} \right]^2 \right\}^{1/2}.$$
 (10)

By defining the depth of focus as that axial distance z_f where the mode diameter differs from its minimum value by 30% [i.e., $\Lambda(z_t) - \Lambda = 0.3\Lambda$], one obtains

$$|z_f| = \frac{0.64\Lambda^2}{\lambda} \sqrt{1 - (2\lambda/\pi\Lambda)^2}.$$
 (11)

For a feature of size $\Lambda = 0.44 \, \mu \text{m}$, which corresponds to the minimum allowed by Eq. (1) for our system, the depth of focus is $\pm 0.35 \, \mu \text{m}$, just within the accuracy of our interferometric focusing procedure.

Figure 5(a) shows a low-resolution micrograph of the photoresist pattern produced by illuminating the entire mask with an expanded laser beam. Each of the 0.8-mm-square chips is a resolution test pattern; the distance between the chips (center of one to center of another) is 2 mm. This exposure (4 h) demonstrates that the usable field size of our device is at least a 6.8-mm square. In later exposures, one chip (lower left corner of pattern) was illuminated by an unexpanded beam and the exposure time was reduced ultimately to 1 min.

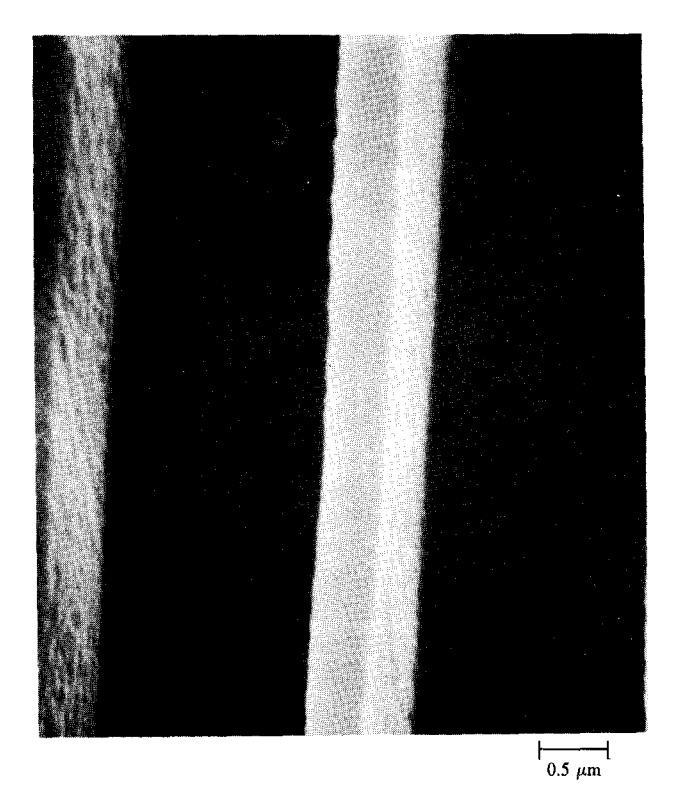


Figure 7 A high-magnification electron micrograph of a vertical wall between two 1.0-µm-wide lines. The wall height is approximately 1.5 µm, as determined by counting standing wave lines.

Figure 5(b) shows a scanning electron micrograph (SEM) of the majority of the pattern formed by the image of one chip. Each of the squares of the checkerboard pattern contains five lines with width and spacing coded by letters. The transparent linewidths increase from 0.5 to 2.0 μ m and the gap widths increase from 0.5 to 4.0 μ m. The inset shows the developed pattern produced by a typical pair of letters which otherwise are not legible in the figure.

High-magnification SEM pictures were taken of all of the line and gap patterns. Figures 6(a) and (b) show two pictures with the finest features, which indicate a maximum transmitted spatial frequency of ≥1000 line pairs per mm. It should be noted that the exposed lines are continuous, without the random gaps expected from an image degraded by laser speckle. Also, there is little or no development in the unexposed regions due to light scattered by dust or scratches on the optics. The image (as weak as it is) is so much brighter than the scattering that speckle due to background illumination by scattered light can be ignored. Some of the irregularity in the image can be attributed to "residual speckle," an interference between the bright image and weak scattering by imperfections in the optics.

Figure 6(c) shows a portion of a developed resist film that was purposely exposed to light diffusely scattered from a ground-glass screen. The rough topography is typical of that produced by speckle. A comparison with Figs. 5 and 6(a, b) verifies the absence of image degradation due to laser speckle.

Figure 7 shows a portion of a vertical wall between two exposed lines. Lines are visible in the wall that result from reduced illumination at the nodes of a standing wave pattern produced by reflection at the resist-substrate interface. Though visible, those lines do not degrade the wall profile. The height of the wall can be measured as 1.5 μ m by counting the nodes which are half a wavelength apart. The width of the wall is 0.4 µm, indicating an aspect ratio of better than 3:1. The depth of focus for lines of varying width can be estimated by measuring the width Λ of the exposed region on the resist on substrates translated by known amounts z from focus. Since a defocused line is likely also to be underexposed and since processing parameters tended to vary a bit from day to day, there are uncertainties in this procedure. Nevertheless, Fig. 8 shows the linewidths A (feature sizes) as measured with a light microscope along with the curve calculated using Eq. (10).

While these experiments in fine-line projection lithography using wavefront conjugation optics seem generally successful, the fact that the focal plane was found to be displaced from the colorless white-light fringe indicates that the magnification is not exactly unity. The 15-µm shift of focus implies that the magnification is actually 1.0007. In fine-line photolithography, magnification variations that large lead to unacceptable overlay difficulties. A beamsplitter cube with higher-quality surfaces, or optics capable of controlling the curvatures of the pump-beam wavefronts should cure this problem.

While these initial results are intriguing, several serious limitations are readily apparent. Most disturbing is that the low brightness of the image requires exposures for minutes for patterning photoresist. The low brightness results partly from the use of a low-power cw laser and partly from the intrinsic low efficiency of our particular conjugator medium. Much higher efficiency can be expected when pulsed lasers are used along with a nonlinear medium where the response is quicker, larger, and not reduced by the transport effects so important in the photorefractive materials. We are presently developing a projection system that uses the third harmonic of a Nd:YAG laser and an absorbing liquid as the nonlinear medium. Adequate exposure should be obtained over a 1-cm² area in 1-2 s.

Conclusions

Wavefront conjugation seems more promising than conventional optics or holography as a means of projecting images

with submicron features. Since most optical aberrations are corrected in the projection process and all surfaces in a conjugator can be plane, the system achieves its full resolution over a large usable field. The depth of focus is no worse than that of a conventional optical system achieving the same resolution, and it can be better if deep uv or vacuum uv wavelengths are used. Neither speckle nor image distortion poses a serious problem and the geometry of a wavefront conjugator facilitates accurate focusing, leveling, and overlay. The prime technical difficulty remaining is the low brightness of the projected image. The use of a powerful pulsed laser and more efficient nonlinear materials should overcome this problem. Electron-beam lithography will be necessary to prepare the 1:1 masks for replication by wavefront conjugation projection photolithography, and for manufacturing certain highly personalized devices, but given sufficient engineering effort, optical lithography by means of wavefront conjugation should fulfill its promise of becoming an important manufacturing technology.

References and note

- R. W. Hellwarth, "Generation of Time-Reversed Wave Fronts by Nonlinear Refraction," J. Opt. Soc. Amer. 67, 1-3 (1977).
 D. M. Bloom and G. C. Bjorklund, "Conjugate Wave-Front
- D. M. Bloom and G. C. Bjorklund, "Conjugate Wave-Front Generation and Image and Construction by Four-Wave Mixing," Appl. Phys. Lett. 31, 592-594 (1977).
- 3. A. Yariv, "Phase Conjugate Optics and Real-Time Holography," *IEEE J. Quantum Electron.* QE-14, 650-660 (1978) and the corresponding erratum in QE-15, 524 (1979).
- 4. M. D. Levenson, "High Resolution Imaging by Wave-Front Conjugation," Opt. Lett. 5, 182-184 (1980).
- M. D. Levenson, K. Johnson, V. C. Hanchett, and K. Chiang, "Projection Photolithography by Wave-Front Conjugation," J. Opt. Soc. Amer. 71, 737-743 (1981).
- B. J. Lin, "Optical Methods for Fine Line Lithography," Fine Line Lithography, Roger Newman, Ed., North-Holland Publishing Co., New York, 1980, pp. 105-232.
- R. G. Brewer, Electron Beam Technology in Microelectronic Fabrication, Academic Press, Inc., New York, 1980.
- 8. See the entire special issue on VLSI, *IEEE Trans. Electron Devices* ED-27, 1319-1725 (1980).
- 9. R. J. Collier, C. B. Burckhardt, and L. H. Lin, Optical Holography, Academic Press, Inc., New York, 1971.
- N. Bloembergen, Nonlinear Optics; A Lecture Note and Reprint Volume, W. A. Benjamin, New York, 1965.
- 11. R. W. Hellwarth, Third Order Nonlinear Susceptibility of Liquids and Solids, Vol. 5 in Progress in Quantum Electronics, Pergamon Press, Oxford, England, 1977.
- J. H. Marburger, "Self-Focusing: Theory," in Vol. 4 of Progress in Quantum Electronics, J. H. Sanders and S. Stenholm, Eds., Pergamon Press, Oxford, England, 1975, pp. 35– 110; also, Y. R. Shen, "Self-Focusing: Experiment," ibid., pp. 1-34.
- M. D. Levenson and J. J. Song, "Coherent Raman Spectroscopy," in Coherent Nonlinear Optics—Recent Advances, M. S. Feld and V. S. Letokhov, Eds., Vol. 21 of Topics in Current Physics, Springer-Verlag, Berlin, 1980, pp. 271-367.
- Herwig Kogelnick, in Modern Optics, J. Fox, Ed., Polytechnical Press, New York, 1977; "Coupled Wave Theory for Thick Hologram Gratings," Bell Syst. Tech. J. 48, 2909-2947 (1969).
- M. J. Beesley, H. Foster, and K. G. Hambleton, "Holographic Projection of Microcircuit Patterns," *Electron. Lett.* 4, 49-50 (1968).

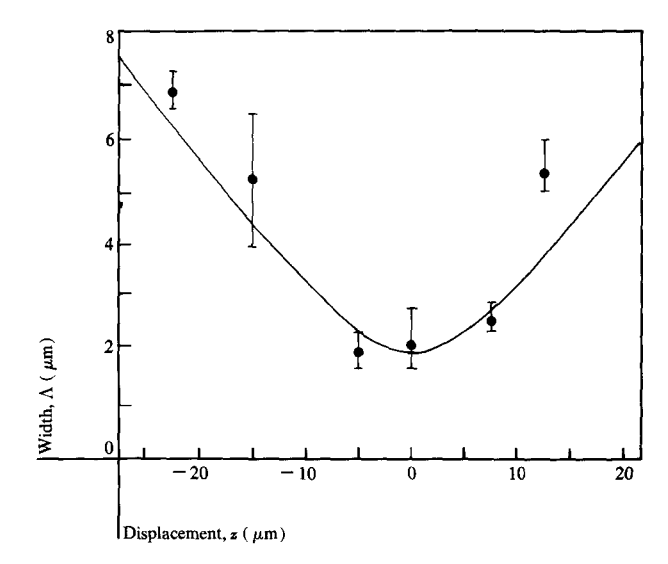


Figure 8 Measured linewidths (feature sizes) Λ for various displacement distances z from the plane of best focus. The solid line corresponds to the predictions of Eq. (10). The data points correspond to observations for lines of 2.0- μ m nominal width. The error bars reflect uncertainties resulting from differences in exposure and developing parameters.

- H. J. Geritsen, W. J. Hannan, and E. G. Ramberg, "Elimination of Speckle Noise in Holograms with Redundancy," Appl. Opt. 7, 2301-2311 (1968).
- J. P. Huignard, J. P. Herrian, L. Pichon, and A. Marrakchi, "Speckle-Free Imaging in Four-Wave Mixing Experiments with Bi₁₂SiO₂₀ Crystals," Opt. Lett. 5, 436-437 (1980).
- J. D. Cuthbert, "Optical Projection Printing," Solid State Technol. 20, 59-69 (1977).
- Daniel Grishkowsky, "Adiabatic Following," in Laser Applications to Optics and Spectroscopy, Vol. 2 of Physics of Quantum Electronics Series, Stephen F. Jacobs, Murray Sargent III, James F. Scott, and Marlan O. Scully, Eds., Addison-Wesley Publishing Co., Inc., Reading, MA, 1975, pp. 437-452.
- R. G. Brewer, "Coherent Optical Spectroscopy," Frontiers in Laser Spectroscopy, Vol. I, R. Balian, S. Haroche, and S. Liberman, Eds., North-Holland Publishing Co., Amsterdam, 1977, pp. 343-396.
- N. Bloembergen and M. D. Levenson, High Resolution Laser Spectroscopy, K. Shimoda, Ed., Vol. 3 of Topics in Applied Physics, Springer-Verlag, Heidelberg, 1976.
- 22. V. S. Letokhov and V. P. Chebotayev, *Nonlinear Spectroscopy*, Springer-Verlag, Berlin, 1977.
- D. G. Steel, R. C. Lind, J. F. Lam, and C. R. Giuliano, "Polarization-Rotation and Thermal Motion Studies via Resonant Degenerate Four-Wave Mixing," Appl. Phys. Lett. 35, 376-379 (1974).
- J. Hubbard, "On the Resolving Power of Time-Reversed Wave Front Imaging Devices," J. Opt. Soc. Amer. 71, 1029-1032 (1981).
- J. T. Hunt, J. P. Glaze, W. W. Simmons, and P. A. Renard, "Suppression of Self-Focusing Through Low Pass Spatial Filtering and Relay Imaging," Appl. Opt. 17, 2053-2057 (1978).
- John H. Marburger and Juan F. Lam, "Effect of Nonlinear Index Changes on Degenerate Four Wave Mixing," Appl. Phys. Lett. 35, 249-251 (1979).
- D. Grishkowsky, N. S. Shiren, and R. J. Bennett, "Generation of Time-Reversed Wave Fronts Using a Resonantly Enhanced Electronic Nonlinearity," Appl. Phys. Lett. 33, 805-807 (1978).

- 28. J. Feinberg, "Real-Time Edge Enhancement Using the Photorefractive Effect," Opt. Lett. 5, 330-332 (1980).
- G. K. L. Wong and Y. R. Shen, "Transient Self-Focusing in a Nematic Liquid Crystal in the Isotropic Phase," Phys. Rev. Lett. 32, 527 (1974).
- D. E. Watkins, J. F. Figueira, and S. J. Thomas, "Observation of Resonance by Enhanced Degenerative Four-Wave Mixing in Doped Alkali Halides," Opt. Lett. 5, 169-171 (1980):
- P. F. Liao and D. M. Bloom, "Continuous-Wave, Backward-Wave Generation by Degenerate Four-Wave Mixing in Ruby," Opt. Lett. 3, 4-6 (1978).
- 32. P. F. Liao, D. M. Bloom, and N. P. Economou, "CW Optical Wave-Front Conjugation by Saturated Absorption in Atomic Sodium Vapor," Appl. Phys. Lett. 32, 813-815 (1978); L. M. Humphrey, J. P. Gordon, and P. F. Liao, "Angular Dependence of Lineshape and Strength of Degenerate Four-Wave Mixing in a Doppler-Broadened System with Optical Pumping," Opt. Lett. 2, 58-60 (1978).
- D. M. Bloom, P. F. Liao, and N. P. Economou, "Observation of Amplified Reflection by Degenerate Four-Wave Mixing in Atomic Sodium Vapor," Opt. Lett. 2, 58-60 (1978).
- P. F. Liao and G. L. Bjorklund, "Polarization Rotation Induced by Resonant Two-Photon Dispersion," *Phys. Rev. Lett.* 36, 584 (1976).
- R. K. Jain, M. B. Klein, and R. C. Lind, "High Efficiency Degenerate Four-Wave Mixing of 1.06-μm Radiation in Silicon," Opt. Lett. 4, 328-330 (1979).

- A. M. Glass, "The Photorefractive Effect," Opt. Eng. 17, 470-479 (1978) and references therein.
- P. W. Smith, A. Ashkin, and W. J. Tomlinson, "Four-Wave Mixing in an Artificial Kerr Medium," *Paper Th12*, p. 54, 1980 Annual Meeting Opt. Soc. of America, Chicago, October 14– 17, 1980; abstract only appears in *J. Opt. Soc. Amer.* 70, 1612 (1980).
- A. Krumins and P. Günter, "Diffraction Efficiency and Energy Transfer During Hologram Formation in Reduced KNbO₃," Appl. Phys. 19, 153-163 (1979).
- 39. *AZ is a registered trademark of the Azoplate Division of American Hoechst Corp., Somerville, NJ 08876.

Received December 29, 1980; revised September 17, 1981

M. D. Levenson is located at the IBM Research Division laboratory, 5600 Cottle Road, San Jose, California 95193. K. Chiang is with the General Optronics Corporation, 3005 Hadley Road, South Plainfield, New Jersey 07080.